A Kinetic Analysis of the Growth and Doping Kinetics of the SiC Chemical Vapor Deposition Process

Carlo Cavallotti,* Filippo Rossi, Stefano Ravasio, and Maurizio Masi

Dipartimento di Chimica, Materiali e Ingegneria Chimica "Giulio Natta", Politecnico di Milano via Mancinelli 7, 20131 Milano, Italy

1. INTRODUCTION

In the last decades, the semiconductor industry has been searching continuously for novel materials to be used for high-tech innovative devices. Among them, silicon carbide (SiC) presents unique characteristics such as a large band gap, high thermal conductivity, high breakdown field, and good corrosion resistance.[1−3] These properties allow the realization of more reliable and smaller devices that are able to work at higher voltages and current densities than possible with other semiconductors. This makes SiC an extremely suitable material for high-power and high-temperature applications.[4,5] Though the growth of SiC has been the object of active research for many years, its use on the industrial scale is still limited by various difficulties, some of them related to the production of high-quality single-crystalline ingots from which the substrates are then cut. Although the possibility of producing large-diameter wafers has been demonstrated, there are still problems in producing ingots with diameters larger than 3−4 in., while the current minimum standard for massive technological development is considered the 6 in. diameter substrate.[6] Moreover, the quality of the substrates available on the market today does not meet the high standard of thickness uniformity and the absence of defects (mainly represented by basal-plane dislocations and micropipes) requested by the microelectronics and semiconductor industry.[5,7] For this reason, and to allow the incorporation of dopants, epitaxial single-crystal layers are usually deposited on the SiC substrates obtained from the SiC ingots. Chemical vapor deposition (CVD) is indeed the only route to industrially perform epitaxial single-crystal SiC growth because of the high temperature involved in the process and the level of control and purity that is required.[5,8] The traditional recipe is based on the use of silane and light hydrocarbons as the Si and C precursors, respectively. Unfortunately, the maximum concentration of gas-phase precursors that can be maintained in this process is determined by the need to avoid the formation of particulates, which nucleate easily even at relatively low SiH_4 concentrations. This requirement thus indirectly imposes a severe upper limit on the film growth rate. To ensure both high-quality films and high-throughput production processes, the use of chlorinated precursors has recently emerged as the most promising route in SiC technology.[1,9]

High-quality models of the deposition process can be extremely useful in order to optimize the SiC deposition process. Such models may be centered either on the fluid dynamics of the CVD reactor or on the kinetics of the growth process.[10−12] One of the first models of the gas-phase kinetics active during the growth of SiC from silanes was developed by Allendorf and Kee,[13] and it was more recently updated by Danielsson et al.[14] The first detailed mechanism of SiC epitaxial single-crystal growth involving chlorinated species was developed by Veneroni and Masi in 2006.[9] It consisted of a model of the gas-phase and surface chemistry active during the deposition of light hydrocarbons, silane, and either chlorosilanes and/or HCl as chlorinated species. In the last years other in silico approaches have been developed with the aim to

Received: November 18, 2013
Revised: January 26, 2014
Accepted: January 27, 2014
Published: January 27, 2014

Table 1. Si−H−Cl Gas-Phase Kinetic Mechanism[a]

reaction	$\log_{10} A$	α	E_a (kcal/mol)	notes
$SiH_3Cl \rightleftarrows H_2 + SiHCl$	14.39	0	68.4	*b*
$SiH_2Cl_2 \rightleftarrows SiHCl + HCl$	14.84	0	75.8	*b*
$Si + HCl \rightleftarrows SiCl + H$	14.98	0	13.6	*c*
$Si + H_2 \rightleftarrows SiH_2$	12.08	0.5	0.	*d*
$SiH_2Cl_2 \rightleftarrows SiCl_2 + H_2$	13.92	0	77.4	*b*
$SiCl_4 \rightleftarrows Cl + SiCl_3$	15.68	0	111.2	*e*
$SiCl_4 + H_2 \rightleftarrows 2HCl + SiCl_2$	7.43	1.94	62.2	*f*
$SiHCl_3 \rightarrow SiCl_2 + HCl$	12.51	0.65	70.4	*g*
reverse	3.69	2.52	14.2	*h*
$SiHCl_3 + HCl \rightarrow SiCl_4 + H_2$	3.34	2.67	42.6	*g*
reverse	6.83	2.11	60.6	*h*
$SiHCl_3 \rightarrow SiCl_3 + H$	17.77	−0.75	93.8	*g*
reverse	13.3	0.08	−0.2	*h*
$SiHCl_3 \rightarrow SiHCl_2 + Cl$	20.54	−1.30	110.4	*g*
reverse	14.53	−0.12	−0.2	*h*
$SiCl_4 \rightarrow SiCl_3 + Cl$	22.84	−1.96	111.6	*g*
reverse	12.95	0.23	−0.4	*h*
$SiH_2Cl_2 \rightarrow SiHCl_2 + H$	17.94	−0.7	93.1	*g*
reverse	13.14	0.18	−0.4	*h*
$Si_2Cl_6 \rightarrow 2SiCl_3$	22.98	−2.15	79.0	*g*
reverse	11.58	0.25	0.2	*h*
$Cl_2HSiSiHCl_2 \rightarrow 2SiHCl_2$	23.70	−2.37	77.7	*g*
reverse	12.43	0.17	0.3	*h*
$Si_2HCl_5 \rightarrow SiCl_3 + SiHCl_2$	23.72	−2.36	78.9	*g*
reverse	11.41	0.43	−0.1	*h*
$SiHCl_2 \rightarrow SiCl_2 + H$	19.11	−1.25	50.3	*g*
reverse	12.86	0.35	−0.7	*h*
$SiCl_3 + HCl \rightarrow SiHCl_3 + Cl$	6.86	1.56	9.5	*g*
reverse	11.26	0.74	0.	*h*
$SiHCl_2 + HCl \rightarrow SiH_2Cl_2 + Cl$	6.9	1.63	9.6	*g*
reverse	11.08	0.94	−0.7	*h*
$SiCl_3 + SiHCl_3 \rightarrow SiCl_4 + SiHCl_2$	4.58	2.66	18.	*g*
reverse	5.18	2.57	17.2	*h*
$SiHCl_2 + SiHCl_3 \rightarrow SiCl_3 + SiH_2Cl_2$	3.70	2.98	6.1	*g*
reverse	3.76	3.04	5.4	*h*
$SiCl_3 + HCl \rightarrow SiCl_4 + H$	2.08	3.08	11.8	*g*
reverse	9.97	1.47	19.0	*h*
$SiHCl_3 + H \rightarrow SiCl_3 + H_2$	8.87	1.60	2.7	*g*
reverse	5.11	2.44	13.9	*h*
$SiHCl_2 + HCl \rightarrow SiHCl_3 + H$	2.38	3.00	12.0	*g*
reverse	9.67	1.48	20.1	*h*
$SiH_2Cl_2 + H \rightarrow SiHCl_2 + H_2$	9.08	1.62	12.0	*g*
reverse	5.34	2.39	14.8	*h*
$Si_2Cl_6 \rightarrow SiCl_2 + SiCl_4$	12.08	0.47	48.3	*g*
reverse	1.57	3.03	13.0	*h*
$Si_2HCl_5 \rightarrow SiCl_2 + SiHCl_3$	11.79	0.48	45.5	*g*
reverse	1.60	3.01	12.0	*h*
$Cl_2HSiSiHCl_2 \rightarrow SiCl_2 + SiH_2Cl_2$	11.11	0.65	48.4	*g*
reverse	1.08	3.16	15.3	*h*
$Cl_3SiSiClH_2 \rightarrow SiCl_2 + SiH_2Cl_2$	11.08	0.66	43.4	*g*
reverse	0.61	3.24	9.4	*h*
$Cl_3SiSiClH_2 \rightarrow SiHCl + SiHCl_3$	10.84	0.62	46.6	*g*
reverse	1.20	2.99	1.8	*h*
$Si_2HCl_5 \rightarrow SiHCl + SiCl_4$	11.18	0.60	51.0	*g*
reverse	2.20	2.93	4.9	*h*
$SiHCl + SiHCl_3 \rightarrow Si_2Cl_4 + H_2$	1.11	3.24	8.0	*g*
reverse	4.11	2.36	6.2	*h*
$Si_2Cl_4 \rightarrow 2SiCl_2$	24.14	−2.92	24.9	*g*
reverse	13.57	−0.23	0.4	*h*

[a]Kinetic constants are high-pressure limits and are expressed as $k = AT^{\alpha} \exp(-E_a/RT)$, with A in units consistent with cm, s, and mol and E_a in kcal/mol. [b]From Su and Schlegel.[39] [c]From Kunz and Roth.[40] [d]From Veneroni and Masi.[9] The rate constant is a collisional value. This reaction has been

Table 1. continued

introduced to enforce the attainment of equilibrium between these species. [e]From Valente et al.[38] [f]From Cavallotti and Masi.[41] [g]From Ravasio et al.[34] [h]The backward rate constant was estimated from detailed balance using CCSD(T) energies calculated with extrapolation to the complete basis set limit and with vibrational frequencies calculated in the harmonic oscillator approximation, except for low-frequency vibrational modes degenerating into rotations, which were treated using a 1D hindered rotor model.[34]

describe the impact of the addition of chlorine precursors on the SiC gas-phase chemistry and growth rate. In particular several kinetic analyses have been performed to investigate the deposition of SiC from different precursors, such as HCl,[9,15] $SiHCl_3$,[3] and CH_3Cl.[16] Recently Leone et al.[2] compared the kinetics of five different silicon precursors (SiH_4, SiH_2Cl_2, $SiHCl_3$, $SiCl_4$, and CH_3SiCl_3), thus allowing further progress of our understanding of the SiC growth process to be obtained. An additional improvement in the modeling of the SiC growth can be obtained through the inclusion of n- and p-doping mechanisms in the kinetic scheme.[16−18] Indeed, because SiC is a semiconductor, it is of high technological interest to grow p-doped and n-doped films by the addition of a controlled amount of the dopant element precursor to the deposition recipe. However, only a few doping models have been reported in the literature, so there is still much to understand in the SiC doping kinetics, particularly in the presence of chlorinated species.[17,19−24]

The purpose of the present study is to present a widespread analysis of the chemical kinetics active during the epitaxial CVD of SiC when chlorine is present in the gas phase, including mechanisms for p and n doping. The specific problems that we address in the present paper include the following: an accurate investigation of the gas-phase reactivity of Si−H−Cl mixtures, which is in our opinion underestimated by the existing models; the identification of the key reactions active during N doping of SiC films, as in our opinion some important reaction channels have not yet been identified; and the proposal of a predictive kinetic model for Al doping in SiC thin films, which is presently missing in the literature. The predictions of the kinetic models presented in this work are compared with experimental results measured in an industrial reactor.[10,25−29]

2. METHOD

Simulations were performed using a 1D model developed by us that has been described in detail in our previous works.[30] Briefly, the model solves the mass and energy conservation equations along the flow direction while the mass and energy transfer to the reactor walls, susceptor, and growth surface are solved using boundary layer theory. The model equations are reported in the Supporting Information, together with a discussion of the expected accuracy of the model. For the experimental runs considered in the present study, the Reynolds number is between 10 and 20, so the growth is always performed in the laminar regime. The mass and energy transfer coefficients are determined using the Luikov expressions for fully developed flows in rectangular ducts.[31] Diffusion and thermal diffusion coefficients are calculated from Lennard-Jones parameters. Because of the high-dilution conditions, the conductivity and viscosity of the gas-phase mixture are assumed to be equal to those of hydrogen. The surface reaction kinetics is solved in the pseudo-steady-state approximation together with the homogeneous mass and energy conservation equations, which makes the problem a differential algebraic one. The numerical integration was performed using the daspk 2.0 solver.[32,33]

The gas-phase and surface kinetics are described using a kinetic mechanism consisting of three parts: the mechanism for SiC deposition from chlorinated species, the n-doping mechanism, and the p-doping mechanism. As most of these mechanisms have been published in the literature, it would be redundant to report and discuss them here explicitly. Thus, most of them are reported in the Supporting Information, while the elements of novelty are discussed in detail for each submechanism in the following.

The SiC mechanism is composed of (i) the mechanism proposed by Danielsson et al.[14] for the gas-phase Si−C−H kinetics, (ii) a part of the Si−H−Cl gas-phase mechanism we developed recently on the basis of ab initio and transition-state theory calculations,[34] and (iii) the surface mechanism for SiC deposition of Veneroni and Masi.[9] The Danielsson mechanism has been slightly modified in regard to the CH_4 decomposition rate constant, for which the high-pressure data of Baulch et al.[35] were used; the rate constants for decomposition of C_2H_4 to C_2H_3 and C_2H_2, for which the data of Baulch et al.[35] were used; and the important rate constant for the reaction between CH_4 and H to give CH_3 and H_2, which rules the equilibrium between the two relevant gas-phase chemical species and for which the accurate estimation of Michael and co-workers[36] was used. Differently from Danielsson et al.,[14] all of the reactions were considered as reversible with backward rate constants determined using detailed balance, except for the hydrogen decomposition rate constant, for which explicit expressions were used for the forward and backward processes to correctly account for third-body efficiencies. In regard to the Si−H part of the Danielsson mechanism, only the SiH_4 decomposition rate constant was changed, as it was substituted with the 0.1 bar value calculated by Barbato et al.[37] using RRKM/master equation simulations. It is noteworthy that this is the only rate constant in the kinetic mechanism for which the pressure dependence has been explicitly taken into account. A preliminary sensitivity analysis of the rate constants that may be in fall off under the considered operating conditions, notably that for the CH_4 unimolecular decomposition, showed that the slowdown effect given by fall off on decomposition rates may impact the simulation results in the first part of the susceptor, in which the temperature changes are most significant, while at the highest temperatures, after the radical reactions have been initiated and the gas phase is mostly at equilibrium, the sensitivity to pressure is reduced. On the whole, it could be concluded that the pressure dependence of the rate constants should be considered if quantitative modeling of the growth rate and doping profiles is needed, while this dependence may be neglected if only average growth rate and concentration values are desired. The Si−C−H mechanism used in the simulations is reported in Table S1 in the Supporting Information.

The Si−H−Cl mechanism we originally proposed,[9] which was based on the study of Valente et al.,[38] was significantly modified with the inclusion of the gas-phase Si−H−Cl mechanism we recently proposed to describe the chlorosilanes' gas-phase reactivity. The mechanism upgrade is likely to lead to a significant enhancement of the gas-phase reactivity of

Table 2. N-Doping Mechanism[a]

reaction	$\log_{10} A$	α	E_a (kcal/mol)	notes
		Gas-Phase Reaction[b]		
$Si_2 + N_2 \rightleftarrows 2SiN$	13.0	0.	0	*c*
		Surface Reactions		
N + \$1 → N*	11.95	0.5	0	*d*, *e*
NNH + 2\$1 → N* + NH*	21.06	0.5	0	*d*, *e*
$2NH^* \rightarrow 2N^* + H_2$	22	0	81.2	*d*
N* + Si* → SiN(b) +\$1	19	0	60	*d*
N* + SiH* → SiN(b) + 0.5H_2 + \$1	19	0	60	*d*
N* + SiH_2* → SiN(b) + H_2 + \$1	19	0	60	*d*
N* + H_2 → NH_2 + \$1	19	0.5	110	*d*
N* + N* → N_2 + 2\$1	19	0	60	*d*
SiCl* + N* → SiN(b) + Cl + \$1 + \$2	19	0	60	*d*
NH_2 + \$1 → NH* + H*	11.92	0.5	0	*d*, *e*
SiN + \$2 → SiN(b) + \$2	11.7	0.5	37	*d*, *f*

[a]Kinetic constants are expressed as $k = AT^{\alpha} \exp(-E_a/RT)$, with A in units consistent with cm, s, and mol and activation energies in kcal/mol. \$1 represents a free Si surface site, while \$2 represents a free C surface site. [b]The mechanism is completed for gas-phase reactions by Table S2 in the Supporting Information. [c]The rate constant is a collisional value. This reaction has been introduced to enforce the attainment of equilibrium between these species. [d]From Fiorucci et al.[20] [e]Collisional with sticking coefficient equal to 1. [f]Collisional with fitted activation energy.

Table 3. Al-Doping Mechanism[a]

reaction	$\log_{10} A$	α	E_a (kcal/mol)	notes
		Gas-Phase Reactions		
$Al(CH_3)_3 \rightarrow Al(CH_3)_2 + CH_3$	15.53	0	76.2	*a*
reverse	12.34	0	0	*a*
$Al(CH_3)_2 \rightarrow AlCH_3 + CH_3$	15	0	39.8	*a*
reverse	12.52	0	0	*a*
$AlCH_3 \rightarrow Al + CH_3$	14.26	0	66.3	*a*
reverse	12.15	0	0	*a*
$AlCH_3 + H \rightarrow Al + CH_4$	14	0	15.1	*a*
reverse	15.43	0	53.4	*a*
AlCl + H → Al + HCl	14	0	17.3	*a*
reverse	14.36	0	3.2	*a*
$AlCl + HCl \rightleftarrows AlCl_2 + H$	−1.328	3.98	5.4	*b*
$AlCl_3 + H \rightleftarrows AlCl_2 + HCl$	8.889	1.63	20.5	*b*
AlH + Cl ⇄ AlCl + H	13	0	0	*b*
AlH + Cl ⇄ Al + HCl	13	0	0	*b*
		Surface Reactions		
Al + \$2 → Al*	11.81	0.5	0	*c*
AlCl + \$2 → AlCl*	11.6	0.5	0	*c*
Al* + C* → AlC(b) + \$1 + \$2	19	0	60	*d*
Al* → Al + \$2	13	0	60	*e*
AlCl* → AlCl + \$2	13	0	30	*d*
Al* + Cl*C → AlCl* + \$1	19	0	25	*f*

[a]Kinetic constants are expressed as $k = AT^{\alpha} \exp(-E_a/RT)$, with A in units consistent with cm, s, and mol and activation energies in kcal/mol. \$1 represents a free Si surface site, while \$2 represents a free C surface site. [a]From Cavallotti et al.[44] [b]From Swihart et al.[47] [c]Collisional. [d]Assumed to be fast. [e]Assumed to be slow. [f]Rate-determining; the activation energy was obtained by fitting of experimental data.

chlorinated species as it contains two different reaction routes, one based on the formation of disilanes as intermediate species and the other on SiH_xCl_y radicals, that are significantly faster than those present in the original mechanism. The Si−H−Cl mechanism used in the simulations is shown in Table 1.

As can be observed, for many reactions the rate constants are explicitly given as forward and backward rate parameters, therefore without enforcing detailed balance. This was done because the rate parameters were calculated using high-level first-principles calculations[34] based on CCSD(T) theory with extrapolation to the infinite basis set, and we felt that for some of the rate parameters the backward rate constants estimated from first principles were more accurate than those that could be determined using the available thermodynamic parameters. This is consistent with the recent finding of Danielsson et al.[42] that the predictions of SiC kinetic models may be significantly affected by the choice of the thermodynamic data set used in the calculations. The surface mechanism used to model the SiC growth is the same described by Veneroni and Masi[9] and is reported in Table S3 in the Supporting Information. As it is well-described in the original paper, it will not be further discussed here, apart from a reminder that it was successfully used to model the growth measured using two different SiC growth reactors in which growth was performed under different operating conditions, thus proving its suitability to simulate different SiC deposition conditions and confirming the

consistency of the chemical and physical assumptions on the basis of which it was developed.

The kernel of the N-doping mechanism was taken from Fiorucci et al.[20] and Meziere et al.,[21] with respect to which it was modified in regard to the addition of one gas-phase reaction and part of the surface mechanism, from which was removed the reaction of dissociative adsorption of N_2. In addition, the rate constant estimated by Caridade et al.[43] was used for the reaction between N_2 and H to give N_2H. The gas-phase mechanism is reported in Table S2 in the Supporting Information, while the surface mechanism and the gas-phase reaction introduced in this work are reported in Table 2. The structure of the mechanism is described in the Results and Discussion, which seemed more appropriate since the motivations behind the modification of the N-doping mechanism originated from a preliminary analysis of the comparison between the simulated and experimental data.

The Al-doping mechanism used for the simulations is presented here for the first time. It is therefore reported fully in its gas-phase and surface parts in Table 3. The mechanism is composed of the gas-phase mechanism for $Al(CH_3)_3$ decomposition proposed by Cavallotti and co-workers[44,45] to describe the gas-phase reactivity active during the AlGaAs deposition process performed in the presence of HCl and of a few selected reactions taken from the computational studies of Swihart and co-workers.[46,47] The reactions taken from the AlGaAs gas-phase kinetic mechanism were estimated using a combination of the kinetic theory of gases and transition-state theory using DFT data determined at the B3LYP level. As explicit rate constants were provided for the forward and backward reactions, detailed balance was not enforced, thus implicitly using the DFT thermochemical parameters. The AlGaAs reaction set describes the decomposition of $Al(CH_3)_3$ into $Al(CH_3)_2$ and $AlCH_3$ and the successive conversion of $AlCH_3$ into Al and AlCl. The conversion of AlCl into $AlCl_2$ and $AlCl_3$ was described introducing a set of four reactions taken form the work of Swihart and co-workers, which were also computed from first principles using transition-state theory.[47] In this case, however, as no explicit expressions for the backward rate constants were given, all of the reactions were considered as reversible, with backward rate constants computed using the NIST−JANAF thermochemical tables.[48] The surface mechanism will be described and discussed in section 3.3.

All of the experimental data reported in this paper were measured in an industrial hot-wall reactor suitable for SiC deposition that was built by LPE, an epitaxial technology company. These data have been published in several different papers in the last years, to which we refer the reader for a detailed description of the measurement methods that were adopted to determine the growth rates and doping levels as well as for details concerning the deposition protocols.[10,25−29] The same reactor was used for all of the depositions, and it is characterized by a reactor height of 2.5 cm and a 21 cm wide susceptor and can accommodate up to six 2 in. wafers and three 3 in. wafers at the same time.[3] The 4H-SiC(0001) wafers are placed on a graphite susceptor, which is 20 cm long and positioned 50 cm from the point of entrance of the gases into the growth chamber. The SiC film and doping precursors are fed into the reactor diluted in a hydrogen carrier gas at a flow rate varying between 100 and 150 slm. The Si precursor was $SiHCl_3$, while the C precursor was C_2H_4. The n-doping precursor was N_2, while $Al(CH_3)_3$ was used for p-doping. All of the depositions were performed at a pressure of 0.1 bar, which enhanced the gas-phase diffusion and slowed the gas-phase reactivity. Doping and growth experiments were performed with susceptor temperatures varying between 1550 and 1650 °C.

3. RESULTS AND DISCUSSION

3.1. SiC Growth Mechanism. The simulations were performed using an imposed temperature profile, which for a susceptor temperature of 1600 °C is shown in Figure 1 together

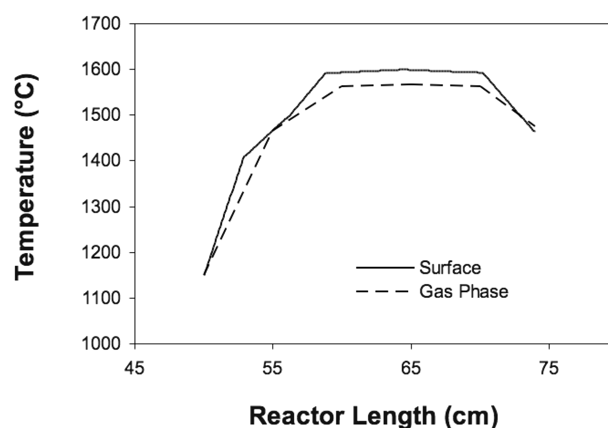

Figure 1. Surface (imposed) and gas-phase (calculated) temperature profiles above the susceptor used in the simulation of SiC growth at a susceptor temperature of 1600 °C.

with the gas-phase temperature computed for a feed of 100 slm H_2. The adopted temperature profile of the deposition surface is expected to give an adequate description of the real temperature distribution on the basis of preliminary calculations that took into account the reactor internal structure and the inductive heating of the susceptor and on the basis of in situ pyrometric measurements of the susceptor temperature profile.

As can be observed, it was assumed that inductive heating of the SiC-coated graphite susceptor will lead to an almost uniform temperature above the substrates, which will however drop rapidly immediately before and after the deposition zone. Also, the gas-phase temperature was calculated to be about 30 °C lower than that of the surface, which, on the basis of full 3D simulations and experimental measurements, is determined by the fact that the hot wall above the susceptor is expected to have a temperature that is about 100 °C lower. This will give rise to a limited temperature gradient above the deposition surface, but in view of the small height of the reactor, this will not considerably affect the diffusion of the precursor through thermal diffusion effects.

The growth rate profile calculated for the given temperature profile using the Si−C−H−Cl mechanism for a feed of 100 slm H_2, 30 sccm $SiHCl_3$, and 22.5 sccm C_2H_4 is shown in Figure 2. The results reported in Figure 2 show that the agreement between the model and experiment is good, although the calculated deposition profile seems to be slightly sharper than that measured experimentally. However, considering the several approximations on which the model is based, most notably the use of a 1D fluid dynamic model rather than a more proper 2D or 3D model, the results may well be considered as satisfactory. An important aspect that was observed while performing a sensitivity analysis of the growth rate over the gas-phase mechanism is that the computation of the backward reactions

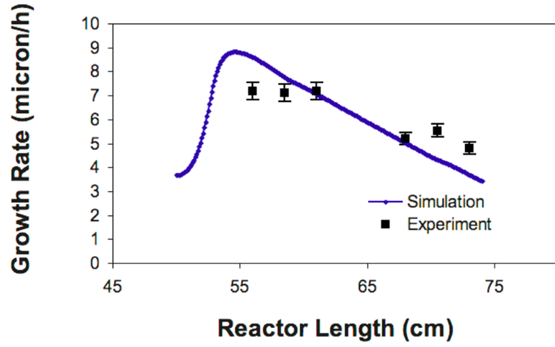

Figure 2. Growth rate calculated using the Si−C−H−Cl mechanism for a feed of 100 slm H_2, 30 sccm $SiHCl_3$, and 22.5 sccm C_2H_4.

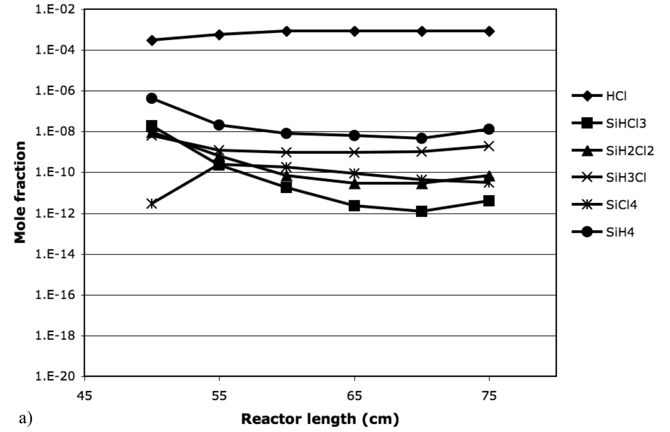

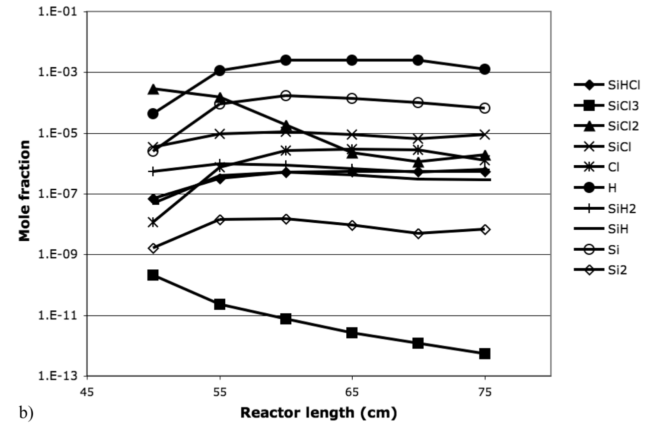

Figure 3. Mole fractions of relevant species above the susceptor for the same conditions as in Figure 2 calculated using the old Si−H−Cl mechanism[9] to describe the conversion of the chlorinated precursors.

of the hydrocarbon chemistry from detailed balance rather than using the explicit expressions given by Danielsson et al.[14] has a non-negligible impact on the growth rate profile, which would be smoother using the Danielsson et al. kinetic mechanism. The reason is that this change in the gas-phase mechanism affects the gas-phase concentration of some of the main SiC carbon precursors, such as methyl and acetylene. Though the difference between the two mechanisms is limited (the deposition profile changes by no more than 20%), this result suggests that some improvement in the hydrocarbon gas-phase mechanism may still be possible.

In order to test the impact that the inclusion of the new Si−H−Cl mechanism we recently developed[34] has on the gas-phase chemistry, two different simulations were performed, one with the original mechanism[9] and the other with the updated mechanism. The concentration profiles computed for the main gas-phase species are shown in Figures 3 (old mechanism) and 4 (new mechanism). As can be observed from a comparison of the two sets of results, the differences are significant for some chemical species, while the concentrations of some key Si growth precursors, such as $SiCl_2$, are almost untouched. The result is that the impact of the new mechanism on the growth rate is almost negligible with the current model, as the concentrations of the main chemical precursors to the film growth are not modified. On the other hand, it can be observed that the gas-phase concentrations of many relevant species are considerably changed.

Comparison of the results obtained using the two kinetic models clearly shows that the original kinetic model, which lacks the radical and disilane conversion pathways, significantly underestimates the gas-phase reactivity. The result is that the extent of $SiHCl_3$ decomposition is overestimated by a factor of 3, the extents of SiH_2Cl_2, and SiH_3Cl formation are underestimated by factors of 20 and 30, and the $SiCl_4$ concentration is overestimated by a factor of about 1000. The reason for this behavior is that the original Si−H−Cl gas-phase model misses some key reaction pathways for the interconversion of the main SiH_xCl_{4-x} chlorinated species. The most relevant pathways introduced by the radical submechanism of the new model are composed by a series of reactions that determine the interconversion of the precursors through a radical chain mechanism. Examples of such reactions are given by the following reaction set:

$$SiHCl_3 \rightarrow SiCl_2 + HCl \qquad (R1)$$

$$SiHCl_3 + SiCl_2 \rightarrow Si_2HCl_5 \qquad (R2)$$

$$Si_2HCl_5 \rightarrow SiCl_3 + SiHCl_2 \qquad (R3)$$

$$SiHCl_3 + SiCl_3 \rightarrow SiCl_4 + SiHCl_2 \qquad (R4)$$

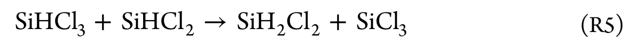

$$SiHCl_3 + SiHCl_2 \rightarrow SiH_2Cl_2 + SiCl_3 \qquad (R5)$$

In reaction R1, $SiHCl_3$ decomposes to give $SiCl_2$ and HCl. Once formed, $SiCl_2$ can react with $SiHCl_3$ to form the Si_2HCl_5 disilane species, which rapidly decomposes to generate two radicals: $SiCl_3$ and $SiHCl_2$. $SiCl_3$ can then react with $SiHCl_3$ to form $SiCl_4$ and $SiHCl_2$, the latter of which can react with another $SiHCl_3$, leading to the formation of SiH_2Cl_2 and $SiCl_3$ and thus closing the $SiCl_3$ catalytic cycle. As the temperature grows, $SiHCl_2$ starts to decompose rapidly in the gas phase (see Figure 4b), thus providing a route to form $SiCl_2$ and atomic H, which can as well lead to the production of $SiCl_3$ through the following two reactions:

$$SiHCl_2 \rightarrow SiCl_2 + H \qquad (R6)$$

$$SiHCl_3 + H \rightarrow SiCl_3 + H_2 \qquad (R7)$$

In parallel to the radical mechanism, conversion between chlorinated Si species can also take place through the disilane mechanism, according to which the system reactivity is enhanced through the formation of intermediate disilane species. An example is given by the following reaction set:

$$SiHCl_3 \rightarrow SiCl_2 + HCl \qquad (R1)$$

$$SiHCl_3 + SiCl_2 \rightarrow Si_2HCl_5 \qquad (R2)$$

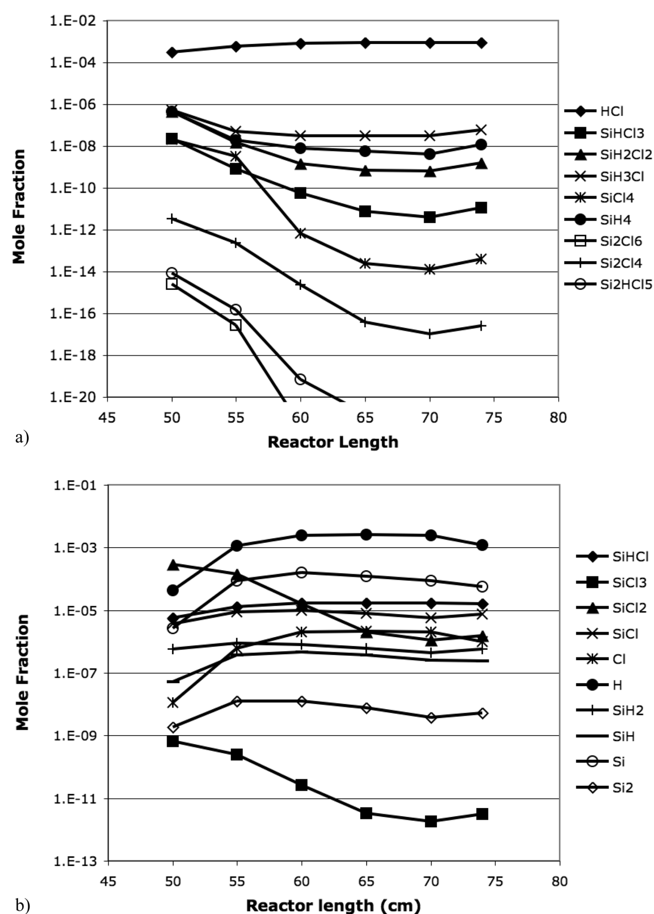

Figure 4. Mole fractions of relevant species above the susceptor for the same conditions as in Figure 2 calculated using the new Si−H−Cl mechanism[34] to describe the conversion of the chlorinated precursors.

$$Si_2HCl_5 \rightarrow SiCl_4 + SiHCl \quad \text{(R8)}$$

$$SiHCl_3 + SiHCl \rightarrow H_2ClSiSiCl_3 \quad \text{(R9)}$$

$$H_2ClSiSiCl_3 \rightarrow SiH_2Cl_2 + SiCl_2 \quad \text{(R10)}$$

The difference between the radical and disilane mechanisms is given by reactions R8−R10, according to which the formation of SiH_2Cl_2 and $SiCl_4$ does not need the formation of an intermediate radical species. According to the simulations we performed in our previous study,[34] these two mechanisms are active contemporarily. For the system under consideration in the present study, however, it is likely that the enhancement of the gas-phase reactivity given by the inclusion of both mechanisms will lead to a gas-phase composition governed by thermodynamic equilibrium. In fact, it can be observed that the concentration of the SiH_xCl_{4-x} gas-phase species follows the order of abundance predicted by thermodynamic equilibrium for chlorosilanes diluted in H_2: $SiH_3Cl > SiH_2Cl_2 > SiHCl_3 > SiCl_4$.[9] As can be observed, this is not the case when simulations neglecting the disilane and radical pathways are performed (Figure 3). In regard to two other key species, SiH_4 and HCl, the two mechanisms predict very similar concentrations, indicating that in both cases the reaction kinetics is sufficiently fast to lead to a substantial equilibrium.

The concentrations of the Si radicals and reactive intermediates generated by the decomposition of the $SiHCl_3$ precursor predicted using the two kinetic models are shown in Figures 3b and 4b. As can be observed, both mechanisms predict that the most abundant active species generated in the gas phase are atomic H and Si. However the mechanisms differ in the prediction of the formation of the third most abundant active species, which is predicted to be $SiCl_2$ by the old mechanism and SiHCl by the updated mechanism. This is a relevant finding, as according to the present simulations SiHCl is together with SiCl and $SiCl_2$ an important Si precursor to the growth of SiC, though the most important contribution comes from atomic Si. The inclusion of atomic Si in the film is controlled by an adsorption/desorption equilibrium that is established at the growth surface. As the growth rate is sensitive to the Si desorption rate, which in the model of Veneroni and Masi[9] was determined through fitting of sublimation pressure data, it is suggested that a higher-level study of this important reaction and of the surface dynamics of atomic Si may lead to a better understanding of the SiC growth mechanism.

As a final remark about the discussion reported here, it is important to point out that the gas-phase reactivity analyzed in this and the following section is significantly influenced by the presence of a reactive surface, which acts as a source or sink of some chemical species. This aspect must thus be considered when extrapolating the results of this study to different systems where the surface may play a less (or more) active role.

3.2. N-Doping Mechanism. The N-doping kinetics was investigated using three different sets of data collected in the same reactor. The first set of data was obtained by measuring N-doping profiles on SiC substrates that were grown using a feed composed of 100 slm H_2, 30 sccm $SiHCl_3$, 22.5 sccm C_2H_4, and 13 sccm N_2. The substrate was maintained at a temperature of 1550 °C.[20] The N-doping mechanism used in the simulations is reported in Table 2 and Table S2 in the Supporting Information. With respect to the N-doping mechanism we previously proposed, this mechanism differs by including in the gas phase a reaction for the formation of the SiN radical, which we propose in the present study to be the main gas-phase precursor for the incorporation of nitrogen in SiC. The motivation to include a new gas-phase reaction and hypothesize that SiN may play a key role in the N-doping mechanism comes from the experimental observation that the N atomic density measured in a SiC film grown in the presence of a gas phase containing N_2 is proportional to the square root of the gas-phase concentration of N_2. This was found for the N-doped films grown using the reactor studied in the present work as well as for a certain N_2 gas-phase concentration range in the experimental study of Forsberg et al.[22] The mechanism we previously proposed to describe the N_2 incorporation kinetics, however, predicts that more than 95% of the nitrogen found in the film comes from dissociative adsorption of N_2 on the SiC film surface. The rate of this reaction is directly proportional to the gas-phase N_2 concentration, which is in contrast with the experimental evidence. To recover the square-root dependence of the N incorporation rate from the N_2 concentration, however, it is sufficient to postulate that the N-doping precursor is a chemical species that is formed in the gas phase with stoichiometric coefficient of 2 from a reaction that reaches equilibrium and in which N_2 appears as a reactant with stoichiometric coefficient of 1. This is for example the case if we postulate that in the gas phase a mechanism is active through which N_2 and atomic Si react to give SiN as a final product. The global reaction for this process would have the following expression:

$$N_2 + 2Si \rightleftarrows 2SiN \quad (R11)$$

The free energy change for this reaction computed at 1500 °C and 1 bar is slightly positive, about 8 kcal/mol, which corresponds to an equilibrium constant of 0.08. This means that, given the relatively high concentrations of N_2 and Si, the equilibrium concentration of SiN will be just a few orders of magnitude smaller than that of Si. Indeed, the simulations revealed that the equilibrium mole fraction of SiN above the susceptor is about 10^{-7}, which is more than sufficient to justify the N atomic densities measured in the film. As reaction R11 is termolecular and thus unlikely from a mechanistic standpoint, it was decided to implement in the model the reaction between disilane and N_2 to give two SiN molecules:

$$Si_2 + N_2 \rightleftarrows 2SiN \quad (R12)$$

If a collisional rate constant of 10^{13} is implemented and the backward rate constant is computed using detailed balance, it is found that this process proceeds rapidly until the equilibrium between the forward and backward processes is reached, at which point the concentration of SiN is proportional to the square root of the product of the concentrations of Si_2 and N_2, thus giving the expected dependence on the N_2 gas-phase concentration. While reaction R12 may be oversimplified in order to describe properly the process of SiN formation, it is however reasonable that at the high temperatures at which this process is performed a fast reaction route leading to the formation of SiN probably exists. It is also here important to point out that the route leading to the formation of SiN may involve the formation of HSiN, which is thermodynamically considerably more stable than SiN, as an intermediate species. Here, however, SiN was considered a more likely precursor to N-doping since, being a radical, it has a much higher reactivity than HSiN. Finally, it is also worth noting that the square-root dependence on the N_2 concentration would be obtained also if the N-doping precursor were any of the species atomic N, NH, NH_2, or NH_3 and if these species were at equilibrium with N_2. However, the reaction mechanism we implemented includes the most known routes for the formation of these species from N_2 in a hydrogen environment, so the negligible calculated concentrations of such species above the susceptor indicates that there is a considerable kinetic limitation to their formation.

The comparison between the calculated experimentally measured N-doping profiles is reported in Figure 5a, while the concentration profiles of the most abundant gas-phase nitrogen species along the susceptor are shown in Figure 5b. The N-doping profile was determined using a SiN incorporation rate having a pre-exponential factor determined from collision theory and an activation energy obtained by fitting of the experimental data. The fitted activation energy is 37 kcal/mol, which indicates that the gas-phase concentration produced at equilibrium for SiN is more than sufficient to account for the measured doping levels. The data in Figure 5b show that the computed mole fraction of SiN in the gas phase is in fact significantly larger than those of all other species that can originate from the reactions of N_2 with hydrogen. Notably, the computed ammonia mole fraction is well below the thermodynamic limit, thus showing that its formation is hindered by kinetic limitations, as pointed out above.

The developed kinetic model was successively used to simulate a second batch and a third batch of experimental data measured from films deposited in the same reactor but under different operating conditions. The growths were performed at

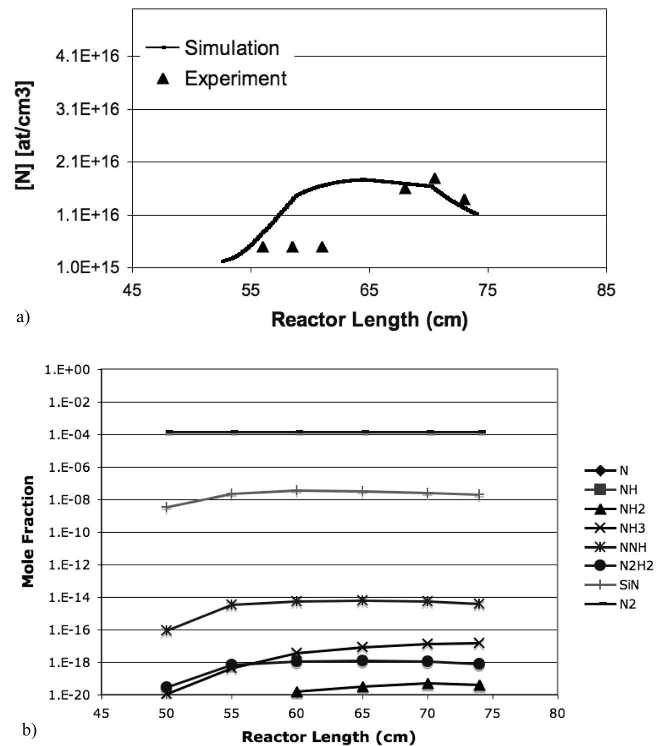

Figure 5. (a) N-doping and (b) gas-phase composition profiles calculated for a deposition performed at a substrate temperature of 1550 °C with a feed composed of 100 slm H_2, 30 sccm $SiHCl_3$, 22.5 sccm C_2H_4, and 13 sccm N_2.

a susceptor temperature of 1650 °C with a $SiHCl_3$ flow rate of 90 sccm. In the first set of experiments, the N_2 flow rate was varied between 80 and 1750 sccm while the C_2H_4 flow rate was fixed at 33.75 sccm; in the second set of experiments, the N_2 flow rate was fixed at 1000 sccm and the C/Si ratio was varied by changing the C_2H_4 flow rate between 27 and 33.75 sccm. The comparisons of the calculated (averaged between 55 and 70 cm, where the substrates are usually positioned) and experimental data[49] for these two different sets of experiments are shown in Figures 6 and 7, respectively. As can be observed,

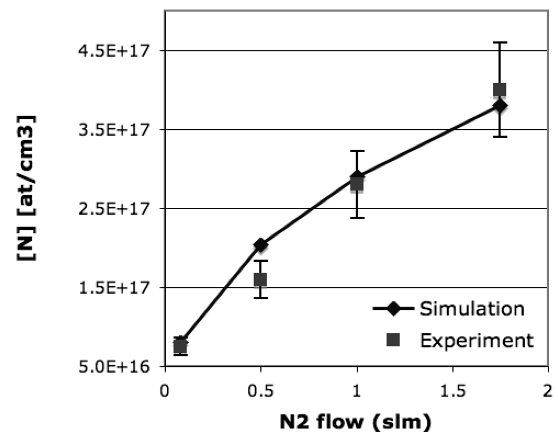

Figure 6. Comparison of the calculated and measured[49] average N-doping levels as a function of the N_2 flow rate on SiC thin films deposited at a susceptor temperature of 1650 °C using a $SiHCl_3$ flow rate of 90 sccm and a C_2H_4 flow rate of 33.75 sccm diluted in 150 slm H_2.

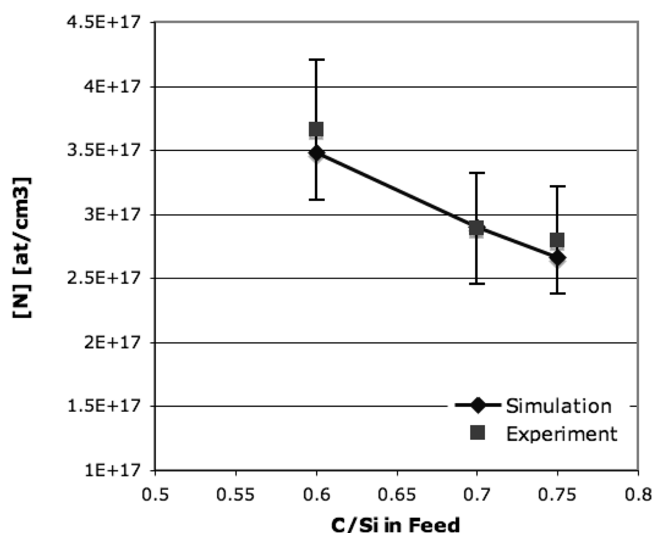

Figure 7. Comparison of the calculated and measured[49] average N-doping levels as a function of the C/Si ratio in the feed on SiC thin films deposited at a susceptor temperature of 1650 °C using a $SiHCl_3$ flow rate of 90 sccm, a N_2 flow rate of 1000 sccm, and a C_2H_4 flow rate varied between 27 and 33.75 sccm, diluted in 150 slm H_2.

the calculated and experimental data are in remarkable agreement, especially considering that no fitting parameters were used. This supports the hypothesis that the N-doping gas-phase precursor is a gas-phase species containing a single N atom that is in equilibrium with N_2.

3.3. Al-Doping Mechanism. The Al-doping mechanism was investigated using the mechanism reported in Table 3. The mechanism was used to simulate data measured in the same reactor adopted to study the N-doping mechanism under similar operating conditions: a susceptor temperature of 1650 °C, a $SiHCl_3$ flow rate of 90 sccm, and a C_2H_4 flow rate of 33.75 sccm, all diluted in 150 slm H_2. The $Al(CH_3)_3$ flow rate was varied between 0.01 and 0.225 sccm. The doping profile calculated for a nonrotating susceptor and the gas-phase concentrations of the main Al-containing gas-phase species are shown in Figure 8a,b, respectively. As can be observed, the Al-doping profile exhibits significant variations along the susceptor length, which would not be acceptable for microelectronic applications. However, it should be remembered that the present simulations were performed in order to enhance the effect of the kinetics without considering the rotation of the susceptor, which would however be activated and would lead to much smoother profiles in case a high-quality film would be desired.

Analysis of the gas-phase composition reveals that, as expected, AlCl is the most abundant gas-phase species, followed by atomic Al, $AlCl_2$, and AlH. The high concentration of atomic Al calculated to be present in the gas phase led us to postulate that, thanks to its high reactivity, it may be the main precursor for incorporation of Al into the film. For this purpose it was assumed that Al may stick on the SiC surface with collisional efficiency and be successively incorporated into the film through a successive surface reaction with a neighboring C* surface species (i.e., a C atom sitting on a Si site). As it was found that this process leads to incorporation of Al in the film that is in excess with respect to the experimental evidence, it was decided to limit the incorporation rate by introducing a reaction through which a surface Cl* species may etch surface Al to give AlCl*, which would then desorb into the gas phase. It

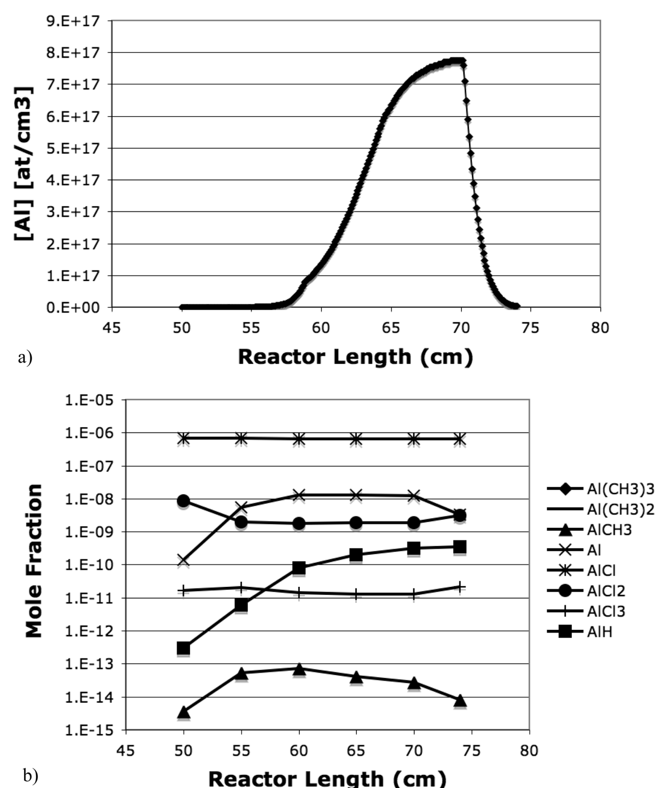

Figure 8. (a) Al-doping profile and (b) gas-phase composition calculated for a deposition performed at a substrate temperature of 1650 °C with a feed composed of 150 slm H_2, 90 sccm $SiHCl_3$, 33.75 sccm C_2H_4, and 0.1 sccm $Al(CH_3)_3$.

was decided to control the Al incorporation in the film using a surface-etching process rather than introducing an activation energy in the sticking coefficient or assuming that Al may desorb into the gas phase, which would give similar results. This choice was dictated by the fact that it was experimentally found that the amount of Al that can be incorporated in a SiC film when the growth is performed in presence of chlorine is significantly smaller than the Al-doping levels that can be obtained in the absence of chlorine,[19,23] thus suggesting that Cl etches Al. The rate constant for the surface-etching process was thus fitted over the experimental data to reproduce the Al-doping levels found at low $Al(CH_3)_3$ flow rates. The fitted activation energy for the Al etching process is 25 kcal/mol. Comparisons of the experimental and simulated data (data labeled as Simulation A) are reported in Figures 9 and 10.

As can be observed, the agreement is good only at low precursor flow rates. This is determined by the fact that at high flow rates the film approaches its Al saturation limit[1] and the Al incorporation rate decreases. The alteration of the kinetics of heavily doped semiconductors is a fact that is well-known in the literature and is often explained in terms of an alteration of the Fermi level of the growth surface.[50] This leads to a modification of the surface reactivity in the direction of a decrease in the rates of the reactions leading to the incorporation of the dopant and of an increase in the rates of the reactions leading to desorption of the dopants that are present on the surface. To prove whether this may be the case, we modified the activation energy for the reaction of etching of surface Al by adsorbed chlorine. We were able to obtain a quantitative fit of the experimental data by decreasing the activation energy for this process by 5 kcal/mol for a $Al(CH_3)_3$ flow rate of 0.225 sccm

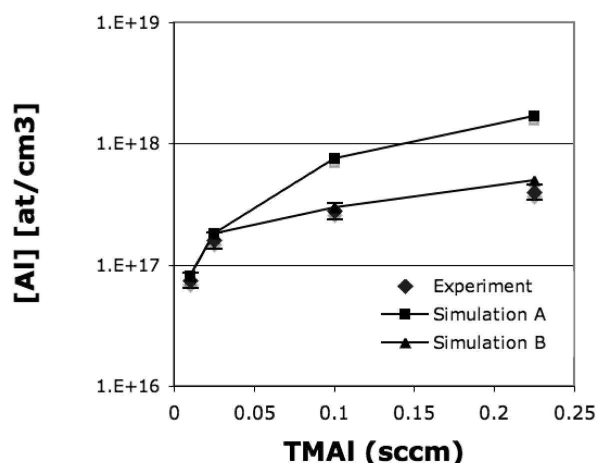

Figure 9. Comparison of the calculated and measured[49] average Al-doping levels as a function of the $Al(CH_3)_3$ flow rate on SiC thin films deposited at a susceptor temperature of 1650 °C using a $SiHCl_3$ flow rate of 90 sccm and a C_2H_4 flow rate of 33.75 sccm diluted in 150 slm H_2.

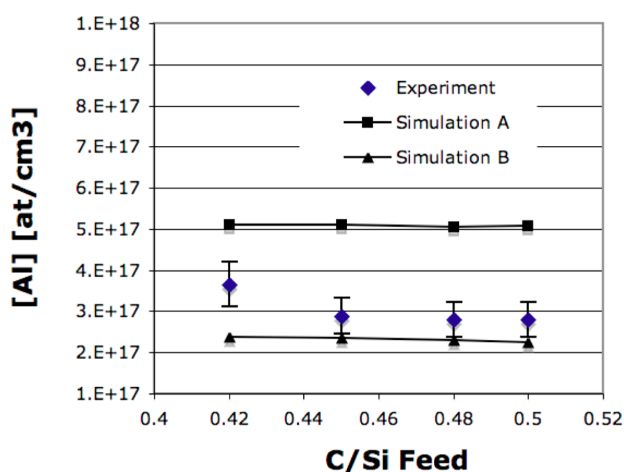

Figure 10. Comparison of the calculated and measured[49] average Al-doping levels as a function of the C/Si ratio in the feed on SiC thin films deposited at a susceptor temperature of 1650 °C using a $SiHCl_3$ flow rate of 90 sccm, a TMAl flow rate of 0.1 sccm, and a C_2H_4 flow rate varied between 18.9 and 22.5 sccm, diluted in 150 slm H_2.

and by 4 kcal/mol for a flow rate of 0.1 sccm. These changes are within the range by which the activation energies of surface reactions can be modified by dopant effects.[50] With the introduction of this modification in the model, it is possible to obtain a quantitative agreement between calculated and experimental data (see the results reported as Simulation B in Figures 9 and 10), but the slightly different trend observed for the dependence of the Al incorporation level on the C/Si ratio in the feed suggests that the surface chemistry may be more complex than described through the present model.

4. CONCLUSIONS

The chemical kinetics active during epitaxial CVD of SiC thin solid films performed in the presence of chlorine has been investigated using a kinetic model composed of a gas-phase and surface mechanism that incorporates two submechanisms able to describe p and n doping. The predictions of the model have been compared with experimental data collected in an industrial reactor produced by LPE. With respect to existing literature kinetic schemes developed to describe the chlorine SiC deposition process, the present model proposes an updated kinetic mechanism for the chlorosilanes' gas-phase reactivity, an update of the n-doping mechanism we proposed a few years ago, and a new model for Al doping in SiC films. The main results of the present kinetic analysis are the following:

(1) The inclusion of the radical and disilane mechanisms in the SiC deposition model considerably enhances the gas-phase reactivity, so the gas-phase composition now approaches the thermodynamic limit. SiH_3Cl is predicted to be the main chlorosilane byproduct, followed by SiH_2Cl_2, $SiHCl_3$, and $SiCl_4$. SiHCl is now predicted to be among the most abundant chemical species that are present in the gas phase, though the main precursor to the film growth is atomic Si. Our simulations predict that the surface kinetics of atomic Si can influence the SiC deposition profile, so it is suggested that its surface reactivity should be investigated in higher detail.

(2) Analysis of the N-doping kinetics suggested that because the N incorporation rate is proportional to the square root of the N_2 partial pressure under the experimental conditions being investigated, the gas-phase kinetics most likely involves a gas-phase decomposition reaction in which N_2 is dissociated to form a chemical species that is in equilibrium with N_2. Here the hypothesis that this chemical species is the SiN radical is advanced. Simulations performed under the assumption that SiN is in equilibrium with N_2 allowed us to obtain a quantitative fit of three different sets of experimental data using as the only fitting parameter the activation energy for inclusion of SiN in the SiC film.

(3) A new kinetic scheme composed of a gas-phase and a surface mechanism is proposed to describe Al doping. It is proposed that the main doping precursor is atomic Al, which is formed in a significant concentration in the gas phase, and that its incorporation into the film is limited by an etching reaction leading to the formation of AlCl, which is assumed to be unreactive on the surface. It is also proposed that the inclusion of Al in the film is limited by an alteration of the surface reactivity that takes place once the Al concentration in the film reaches a critical threshold.

To conclude, we believe that the kinetic schemes proposed here may be used as valuable tools to model the epitaxial SiC deposition process in any CVD reactor. The present mechanism may be used to model processes taking place on substrates with surface temperatures between 1550 and 1650 °C in reactors operating at pressures between 0.1 and 1 bar, which are the operating conditions over which some key parameters of the kinetic model have been fitted.

■ AUTHOR INFORMATION

Corresponding Author

*Tel: ++39-02-23993176. Fax: ++39-02-23993180. E-mail: carlo.cavallotti@polimi.it.

Notes

The authors declare no competing financial interest.

■ ACKNOWLEDGMENTS

This paper is dedicated to Massimo Morbidelli, who was a mentor to all of us. We thank LPE for sharing with us their industrial data.

■ REFERENCES

(1) Pedersen, H.; Leone, S.; Kordina, O.; Henry, A.; Nishizawa, S.; Koshka, Y.; Janzen, E. Chloride-based CVD growth of silicon carbide for electronic applications. *Chem. Rev.* **2012**, *112* (4), 2434−2453.
(2) Leone, S.; Kordina, O.; Henry, A.; Nishizawa, S.; Danielsson, O.; Janzen, E. Gas-phase modeling of chlorine-based chemical vapor deposition of silicon carbide. *Cryst. Growth Des.* **2012**, *12* (4), 1977−1984.
(3) Veneroni, A.; Omarini, F.; Moscatelli, D.; Masi, M.; Leone, S.; Mauceri, M.; Pistone, G.; Abbondanza, G. Modeling of epitaxial silicon carbide deposition. *J. Cryst. Growth* **2005**, *275* (1−2), E295−E300.
(4) Willander, M.; Friesel, M.; Wahab, Q. U.; Straumal, B. Silicon carbide and diamond for high temperature device applications. *J. Mater. Sci.: Mater. Electron.* **2006**, *17* (1), 1−25.
(5) Crippa, D.; Masi, M.; Rode, D. L., *Silicon Epitaxy*; Academic Press: San Diego, CA, 2001.
(6) Kalered, E.; Pedersen, H.; Janzén, E.; Ojamäe, L. Adsorption and surface diffusion of silicon growth species in silicon carbide chemical vapour deposition processes studied by quantum-chemical computations. *Theor. Chem. Acc.* **2013**, *132* (12), No. 1403.
(7) Kimoto, T.; Itoh, A.; Matsunami, H. Step-controlled epitaxial growth of high-quality SiC layers. *Phys. Status Solidi B* **1997**, *202* (1), 247−262.
(8) Hitchmann, M. L.; Jensen, K. F., *Chemical Vapor Deposition: Principles and Applications*; Academic Press: London, 1993.
(9) Veneroni, A.; Masi, M. Gas-phase and surface kinetics of epitaxial silicon carbide growth involving chlorine-containing species. *Chem. Vap. Deposition* **2006**, *12* (8−9), 562−568.
(10) Camarda, M.; La Magna, A.; Severino, A.; La Via, F. Extended study of the step-bunching mechanism during the homoepitaxial growth of SiC. *Thin Solid Films* **2010**, *518*, S159−S161.
(11) Masi, M.; Di Stanislao, M.; Veneroni, A. Fluid-dynamics during vapor epitaxy and modeling. *Prog. Cryst. Growth Charact. Mater.* **2003**, *47* (2−3), 239−270.
(12) Barbato, A.; Cavallotti, C. Challenges of introducing quantitative elementary reactions in multiscale models of thin film deposition. *Phys. Status Solidi B* **2010**, *247* (9), 2127−2146.
(13) Allendorf, M. D.; Kee, R. J. A model of silicon carbide chemical vapor deposition. *J. Electrochem. Soc.* **1991**, *138* (3), 841−852.
(14) Danielsson, O.; Henry, A.; Janzen, E. Growth rate predictions of chemical vapor deposited silicon carbide epitaxial layers. *J. Cryst. Growth* **2002**, *243* (1), 170−184.
(15) Masi, M.; Veneroni, A.; Fiorucci, A.; La Via, F.; Foti, G.; Mauceri, M.; Leone, S.; Pistone, G.; Condorelli, G.; Abbondanza, G.; Valente, G. L.; Crippa, D. Film morphology and process conditions in epitaxial silicon carbide growth via chlorides route. *Mater. Sci. Forum* **2007**, *556−557*, 93−96.
(16) Fiorucci, A.; Moscatelli, D.; Masi, M. Homoepitaxial silicon carbide deposition processes via chlorine routes. *Surf. Coat. Technol.* **2007**, *201* (22−23), 8825−8829.
(17) Fiorucci, A.; Moscatelli, D.; Masi, M. p-Doping mechanism in HTCVD silicon carbide. *J. Cryst. Growth* **2007**, *303* (1), 349−351.
(18) Danielsson, O.; Forsberg, U.; Janzen, E. Predicted nitrogen doping concentrations in silicon carbide epitaxial layers grown by hot-wall chemical vapor deposition. *J. Cryst. Growth* **2003**, *250* (3−4), 471−478.
(19) Pedersen, H.; Beyer, F. C.; Henry, A.; Janzen, E. Acceptor incorporation in SiC epilayers grown at high growth rate with chloride-based CVD. *J. Cryst. Growth* **2009**, *311* (13), 3364−3370.
(20) Fiorucci, A.; Moscatelli, D.; Masi, M. Mechanism of n-doping of silicon carbide epitaxial films. *J. Cryst. Growth* **2007**, *303* (1), 345−348.
(21) Meziere, J.; Ucar, M.; Blanquet, E.; Pons, M.; Ferret, P.; Di Cioccio, L. Modeling and simulation of SiC CVD in the horizontal hot-wall reactor concept. *J. Cryst. Growth* **2004**, *267* (3−4), 436−451.
(22) Forsberg, U.; Danielsson, O.; Henry, A.; Linnarsson, M. K.; Janzen, E. Nitrogen doping of epitaxial silicon carbide. *J. Cryst. Growth* **2002**, *236* (1−3), 101−112.
(23) Forsberg, U.; Danielsson, O.; Henry, A.; Linnarsson, M. K.; Janzen, E. Aluminum doping of epitaxial silicon carbide. *J. Cryst. Growth* **2003**, *253* (1−4), 340−350.
(24) Nishizawa, S.-i.; Pons, M. Growth and doping modeling of SiC-CVD in a horizontal hot-wall reactor. *Chem. Vap. Deposition* **2006**, *12* (8−9), 516−522.
(25) Camarda, M.; Canino, A.; La Magna, A.; La Via, F.; Feng, G.; Kimoto, T.; Aoki, M.; Kawanowa, H. Structural and electronic characterization of (2, 3_3) bar-shaped stacking fault in 4H-SiC epitaxial layers. *Appl. Phys. Lett.* **2011**, *98* (5), No. 051915.
(26) Camarda, M.; La Magna, A.; Fiorenza, P.; Giannazzo, F.; La Via, F. Defect formation and evolution in the step-flow growth of silicon carbide: A Monte Carlo study. *J. Cryst. Growth* **2008**, *310* (5), 971−975.
(27) Camarda, M.; La Magna, A.; Fiorenza, P.; Izzo, G.; La Via, F. Theoretical Monte Carlo study of the formation and evolution of defects in the homoepitaxial growth of SiC. *Mater. Sci. Forum* **2009**, *600−603*, 135−138.
(28) Camarda, M.; La Magna, A.; La Via, F. A kinetic Monte Carlo method on super-lattices for the study of the defect formation in the growth of close packed structures. *J. Comput. Phys.* **2007**, *227* (2), 1075−1093.
(29) Severino, A.; Camarda, M.; Condorelli, G.; Perdicaro, L. M. S.; Anzalone, R.; Mauceri, M.; La Magna, A.; La Via, F. Effect of the miscut direction in (111) 3C-SiC film growth on off-axis (111)Si. *Appl. Phys. Lett.* **2009**, *94* (10), No. 101907.
(30) Masi, M.; Cavallotti, C.; Radaelli, G.; Carra, S. Kinetics of indium phosphide epitaxial growth using metal organic precursors. *Cryst. Res. Technol.* **1997**, *32* (8), 1125−1136.
(31) Luikov, A. V., *Heat and Mass Transfer*; Mir: Moscow, 1980.
(32) Brown, P. N.; Hindmarsh, A. C.; Petzold, L. R. Using Krylov methods in the solution of large-scale differential-algebraic systems. *SIAM J. Sci. Comput.* **1994**, *15* (6), 1467−1488.
(33) Brown, P. N.; Hindmarsh, A. C.; Petzold, L. R. Consistent initial condition calculation for differential-algebraic systems. *SIAM J. Sci. Comput.* **1998**, *19* (5), 1495−1512.
(34) Ravasio, S.; Masi, M.; Cavallotti, C. Analysis of the gas phase reactivity of chlorosilanes. *J. Phys. Chem. A* **2013**, *117* (25), 5221−5231.
(35) Baulch, D. L.; Cobos, C. J.; Cox, R. A.; Frank, P.; Hayman, G.; Just, T.; Kerr, J. A.; Murrells, T.; Pilling, M. J.; Troe, J.; Walker, R. W.; Warnatz, J. Evaluated kinetic data for combustion modeling. Supplement I. *J. Phys. Chem. Ref. Data* **1994**, *23* (6), 847−1033.
(36) Sutherland, J. W.; Su, M. C.; Michael, J. V. Rate constants for H + CH_4, CH_3 + H_2, and CH_4 dissociation at high temperature. *Int. J. Chem. Kinet.* **2001**, 33 (11), 669−684.
(37) Barbato, A.; Seghi, C.; Cavallotti, C. An *ab initio* Rice−Ramsperger−Kassel−Marcus/master equation investigation of SiH_4 decomposition kinetics using a kinetic Monte Carlo approach. *J. Chem. Phys.* **2009**, *130* (7), No. 074108.
(38) Valente, G.; Cavallotti, C.; Masi, M.; Carra, S. Reduced order model for the CVD of epitaxial silicon from silane and chlorosilanes. *J. Cryst. Growth* **2001**, *230* (1−2), 247−257.
(39) Su, M. D.; Schlegel, H. B. An ab initio MO study of the thermal decomposition of chlorinated monosilanes, $SiH_{4-n}Cl_n$ (n = 0−4). *J. Phys. Chem.* **1993**, *97* (39), 9981−9985.
(40) Kunz, A.; Roth, P. A shock tube study of the reaction of Si atoms with HCl. *Phys. Chem. Chem. Phys.* **2000**, *2* (2), 221−226.
(41) Cavallotti, C.; Masi, M. Kinetics of $SiHCl_3$ chemical vapor deposition and fluid dynamic simulations. *J. Nanosci. Nanotechnol.* **2011**, *11* (9), 8054−8060.

(42) Danielsson, Ö.; Sukkaew, P.; Ojamäe, L.; Kordina, O.; Janzén, E. Shortcomings of CVD modeling of SiC today. *Theor. Chem. Acc.* **2013**, *132* (11), No. 1398.
(43) Caridade, P. J. S. B.; Rodrigues, S. P. J.; Sousa, F.; Varandas, A. J. C. Unimolecular and bimolecular calculations for HN_2. *J. Phys. Chem. A* **2005**, *109* (10), 2356−2363.
(44) Cavallotti, C.; Lengyel, I.; Nemirovskaya, M.; Jensen, K. F. A computational study of gas-phase and surface reactions in deposition and etching of GaAs and AlAs in the presence of HCl. *J. Cryst. Growth* **2004**, *268* (1−2), 76−95.
(45) Cavallotti, C.; Nemirovskaya, M.; Jensen, K. F. A multiscale study of the selective MOVPE of $Al_xGa_{1-x}As$ in the presence of HCl. *J. Cryst. Growth* **2003**, *248*, 411−416.
(46) Swihart, M. T.; Catoire, L. Thermochemistry of aluminum species for combustion modeling from ab initio molecular orbital calculations. *Combust. Flame* **2000**, *121* (1−2), 210−222.
(47) Swihart, M. T.; Catoire, L.; Legrand, B.; Gokalp, I.; Paillard, C. Rate constants for the homogeneous gas-phase Al/HCl combustion chemistry. *Combust. Flame* **2003**, *132* (1−2), 91−101.
(48) Chase, M. W.; Davies, C. A.; Downey, J. R.; Frurip, D. J.; McDonald, R. A.; Syverud, A. N. JANAF Thermochemical Tables, 3rd edition. 0.1. AL-CO. *J. Phys. Chem. Ref. Data* **1985**, *14* (Suppl.1), 1−926.
(49) Condorelli, G.; Mauceri, M.; Pistone, G.; Perdicaro, L. M. S.; Abbondanza, G.; Portuese, F.; Valente, G. L.; Crippa, D.; Giannazzo, F.; La Via, F. Thin SiC-4H epitaxial layer growth by trichlorosilane (TCS) as silicon precursor with very abrupt junctions. *Mater. Sci. Forum* **2009**, *600−603*, 127−130.
(50) Masi, M.; Zonca, R.; Carra, S. Kinetic modeling and dopant effect on silicon deposition—Low pressure and plasma assisted chemical vapor deposition. *J. Electrochem. Soc.* **1999**, *146* (1), 103−110.